



## Study on the photovoltaic characteristics of solar cells based on PbS quantum dots and carbon counter electrode

Zafar Ali<sup>\*</sup>, Muhammad Hassan Sayyad, Ahmad Ali, Mujeeb ur Rahman, Nadia Anwar, Sajid Khan

*Faculty of Engineering Sciences, Ghulam Ishaq Khan Institute of Engineering Sciences and Technology, Topi, District Swabi, Khyber Pakhtunkhwa 23640, Pakistan*



### ARTICLE INFO

**Keywords:**  
 QDSSCs  
 lead sulfide (PbS)  
 Successive ionic layer adsorption and reaction (SILAR)  
 Polysulfide  
 Impedance spectroscopy  
 HBM modal

### ABSTRACT

Lead sulfide (PbS) quantum dots (QDs) with their customizable and precise energy levels, have emerged as highly promising photosensitizers in quantum dots sensitized solar cells (QDSSCs). This research focuses on fabricating high-performance QDSSCs anchored on PbS QDs sensitized mesoporous titania coated FTO electrodes. The PbS QDs were grown on mesoporous TiO<sub>2</sub> through the Successive Ionic Layer Absorption and Reaction (SILAR) method. The optical properties were analyzed using UV-visible absorption spectroscopy, revealing that the SILAR cycles impacted the size and band gap of the PbS QDs. By analyzing the absorption data and the hyperbolic band model (HBM), the size of the PbS QDs were estimated to be 1.65 nm, 2.126 nm, 2.326 nm, 2.5692 nm, and 3.048 nm for 1 to 5 SILAR cycles, respectively. The effect of SILAR cycles was investigated, demonstrating a direct correlation between the number of SILAR cycles and the photovoltaic performance of the device. The maximum power conversion efficiency of 2.07 % was attained using 2 SILAR cycles, in contrast to 1.33 % and 1.63 % obtained with one and three SILAR cycles, respectively. Furthermore, impedance spectroscopy (IS), (C<sub>s</sub>-V) (R<sub>s</sub>-V) was employed at different frequencies, highlighting lowest series resistance for 2 SILAR cycles confirming its highest photovoltaic performance. Moreover, The utilization of a low-cost polysulfide electrolyte and carbon electrode has yielded superior or comparable outcomes compared to previously reported data.

### 1. Introduction

Non-renewable energy sources such as burning fossil fuels are the primary methods used to meet the substantial global energy demand. However, the utilization of fossil fuels is hindered by two significant challenges, their finite supply, and the environmental consequences. This compels humanity to seek alternative, sustainable, and long-term futuristic energy solutions [1]. In this regard, Renewable energy sources are the best backup for non-renewable energy sources. The importance of renewable energy (RE) lies in its capability to combat against climate changes, enhance energy bank, sustainable development, Eco-friendly, reduction of CO<sub>2</sub> emissions, flexible energy system as well as its economic potential makes it more suitable for the world modern lifestyle [2]. Solar energy is one of the rich renewable energy sources, to convert sun energy into electrical energy, solar cells are fabricated. The first solar cell was silicon-based with conversion efficiency of 6 % design by Fuller and Gerald [3]. Silicon cells are nowadays mostly utilized for commercial purposes, because of their high efficiency and long lifetime

[4]. But it has certain limitations such as costly, heavy, envelope a large surface area as well as lot of engineering work is required [4–6]. These shortcomings are overcome by solution processable photovoltaic devices such as dye sensitized solar cells (DSSCs), perovskite solar cells (PCs) and quantum dots sensitized solar cells (QDSSCs), having different sensitizing material such as dye, perovskite, and quantum dots material, respectively.

DSSCs were first introduced in the early 1990 s by Gratzel [7] as an innovative technology. Light energy is absorbed by the sensitizer, creating electron-hole pair, the transfer of excited electron to the external load through semiconducting material typically (TiO<sub>2</sub>) constitutes electric current. These types of cells are cost effective, flexible and can work under diffuse light [7]. But their low efficiency and stability hinder its commercialization. Perovskite solar cells (PSCs) on the other hand use perovskite material as absorbing layer to assemble device. PSCs demonstrate elevated conversion efficiency of about 25 %, in addition to, are light weight and flexible and are active area of research [8]. However, several challenges should be addressed like stability,

\* Corresponding author.

E-mail address: [alizafartaj@gmail.com](mailto:alizafartaj@gmail.com) (Z. Ali).

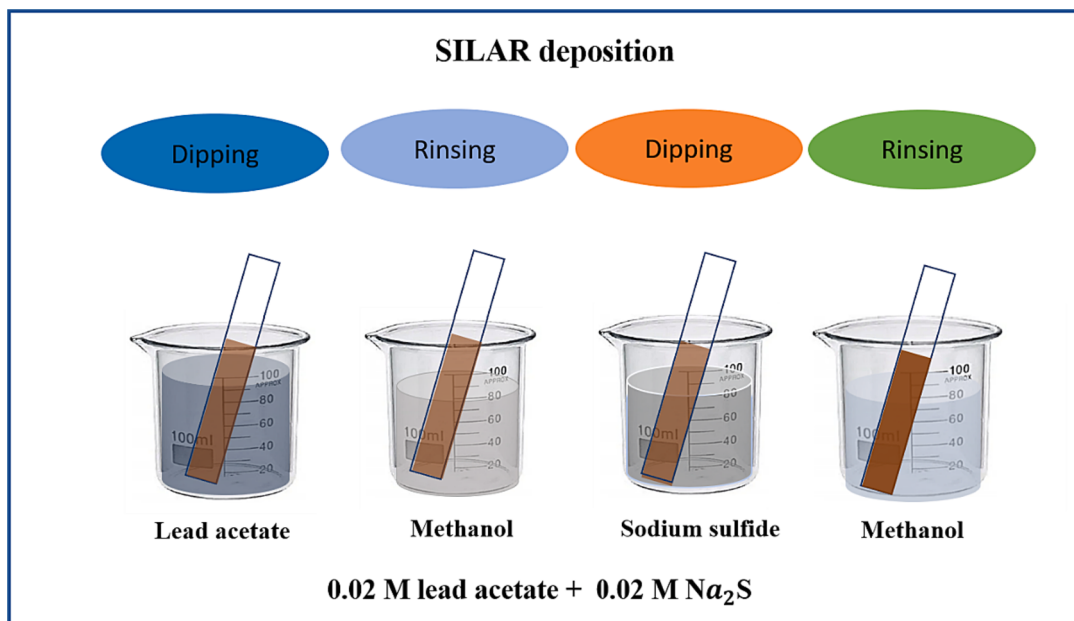


**Fig. 1.** Schematic illustration of synthesis of lead sulfide QDs via SILAR cycles, picture of the prepared samples.

manufacturing methods and durability, to become viable and reliable commercially.

Quantum dots sensitized solar cells (QDSSCs) employ quantum dots material as an absorber layer and can be utilized as an alternative to conventional photovoltaic devices. Quantum dots are nanoscale, direct band gap semiconducting particles and is an intensive area of research to fabricate QDSSCs, attributed to its unique optical and optoelectronic properties likewise, size dependent tunable band gap, outstanding photostability, high absorption coefficient, low cost, and ability to generate multiple excitons [9–11]. QDSSCs are based on the principle of utilizing quantum dots (QDs) as light-absorbing materials replacing the conventional dyes in DSSCs, to harvest light energy and generate electrical energy. Several QDs materials can harvest a wide spectrum of solar energy due to their tunable band gap feature, enabling them to absorb solar radiation both in visible and infrared regions. This characteristic has the potential to break the theoretical limitations and can significantly reach efficiency above 40 % [12]. Furthermore, QDSSCs offers superior charge transport properties, scalable and low-cost solution processable fabrication [13].

Lead sulfide (PbS) is a narrow direct band gap nanoscale semiconducting material with band gap of 0.41 eV in its bulk form, composed of lead and sulfur [14]. Because of their small size, PbS exhibits quantum confinement effect leading to size dependent energy band gap characteristics. PbS can harvest the light in near infrared region and visible

region associated to its tunability making them promising contender for solar energy conversion [15]. Moreover, the electron transport layer, counter electrode, electrolyte, and sensitizer play pivotal roles as fundamental components in solar cells. Presently, there is active research dedicated to developing low-cost, high-performance solar cells. To achieve this objective, it is necessary to reduce the cost of key components. For instance, expensive sensitizing dyes, platinum electrodes, and electrolytes can be replaced with cost-effective alternatives such as quantum dots (QDs), carbon electrodes, and polysulfide electrolytes, respectively. Additionally, the adoption of a simple and inexpensive synthesis technique is highly desirable. SILAR is the simplest deposition technique, relies on successive reactions taking place on the surface of oxides, the process involves rinsing after each reaction, promoting a heterogeneous interaction between the ions in the solution and the solid phase [16,17]. The SILAR method is characterized by its simplicity, controlled growth rate at atomic level via varying SILAR cycles, cost-effectiveness, and compatibility with low-temperature requirements, making it capable of providing uniform coatings. Nonetheless, it does have drawbacks, including a relatively slow growth rate and restrictions on certain types of materials [18]. The SILAR mechanism reveals that the performance of Quantum Dot Solar Cells (QDSCs) is significantly influenced by both the quantity and size of the adsorbed Quantum Dots (QDs) [19]. Due to their diminutive size, PbS displays a quantum confinement effect, resulting in size-dependent energy band

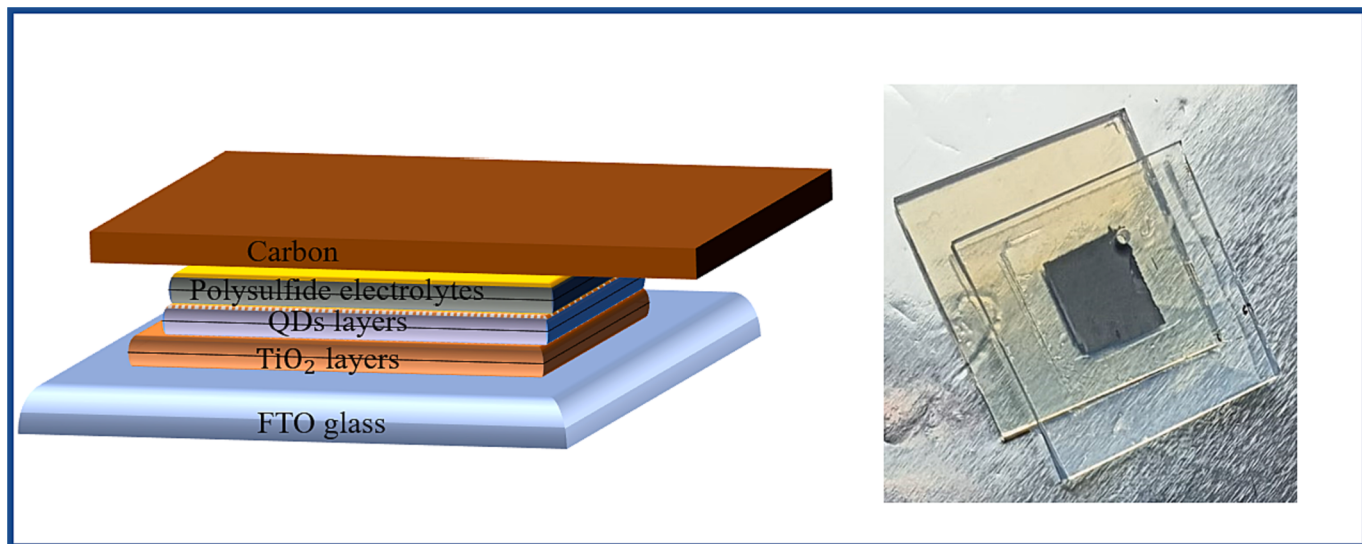


**Fig. 2.** Displaying different layers of device through block diagram, picture of the assembled device.

gap properties. In this regard, Yindeesuk et al. employed PbS as a sensitizer in QDSSCs, illustrating a direct correlation between the SILAR cycle, quantum dot size, and band gap, achieving an efficiency of 1.79 % and a high photocurrent of 16.39 mA/cm<sup>2</sup> [1]. Likewise, SILAR cycles can be employed to synthesize PbS for various technologies, including supercapacitors. Therefore, Pandit et al. conducted the preparation of a composite consisting of Bi<sub>2</sub>S<sub>3</sub>:PbS on MWCNTs using SILAR cycles for the purpose of fabricating a symmetric supercapacitor [20]. Nikam et al. employed the SILAR method for the synthesis of Bi<sub>2</sub>S<sub>3</sub> nanoparticles. Their research focused on characterizing the inorganic semiconductor and exploring its application in solar cell fabrication [21].

In the case of PbS, when both the lead and sulfur source are brought together in the reaction mixture, resulting in precipitation reaction. Sulfur combines with lead to form solid PbS QDs [22].

This research aims to examine how the utilization of SILAR cycles affects the photovoltaic performance of PbS quantum dot solar cells (QDSSCs). The titania electrode was sensitized with lead sulfide quantum dots via SILAR method to prepare photoanode. Corban was used as counter electrode with the photoanode to fabricate the device while sandwiching polysulfide liquid electrolyte between them. Impedance spectroscopies were employed to compare capacitance and resistance of devices. Furthermore, the prepared photoanodes were sensitized for one to five SILAR cycles, revealing highest absorption and efficiency, at three and two SILAR cycles, respectively.

## 2. Experimental methods

### 2.1. Materials

All the fabricating components such as Transparent FTO electrodes with compact, mesoporous, and scattering layer of TiO<sub>2</sub>, Titanium dioxide (TiO<sub>2</sub>) paste, predrilled bare FTO electrodes (10 x 10 mm) gaskets, glass slides, sealings, and caps were purchased from Solaronix, Switzerland.

### 2.2. Chemicals

Lead acetate trihydrate Pb (CH<sub>3</sub>COO)<sub>2</sub>·3H<sub>2</sub>O sodium sulfide trihydrate (Na<sub>2</sub>S·3H<sub>2</sub>O), potassium chloride (KCl), Sulphur (S) as well as solvents and cleaning agents such as methanol, ethanol, and acetone, were all acquired from sigma Aldrich with high purity.

### 2.3. Preparation of glass slides for UV-VIS spectroscopy

The glass slides were cut to the desired size and subsequently underwent a sequential cleaning process in an ultrasonic bath. Each slide was immersed in acetone, IPA, and deionized water for 10 min consecutively. After successful cleaning, Titania paste was coated on the glass substrate by doctor blading technique and fired the substrate at 450 °C for 30 min and gradually cool it to the room temperature, to avoid any cracks due to abrupt change in temperature and get good electrical contact between nanoparticles. QDs were grown on prepared substrate via SILAR process which will be discussed below in detail, and the samples are ready for UV-VIS spectra.

### 2.4. Preparation of PbS QD-sensitized photoanode

Titania coated FTO glass substrates were sintered at 450°C for 30 min and gradually cool it to the room temperature, to prevent cracks caused by sudden temperature changes and to ensure proper electrical contact between the nanoparticles. The prepared titania film substrate was sensitized with PbS QDs via SILAR method. This technique, well described in previous works, involves the crystal growth “layer by layer” by sequentially dipping the substrates into the ionic precursor solutions for 1 min. Firstly, TiO<sub>2</sub> film was dipped for 1 mint into precursor solution of Pb<sup>+2</sup> containing 0.02 M (molar concentration) of lead acetate trihydrate in methanol solvent. Followed by rinsing in methanol to remove the extra unadsorbed Pb<sup>+2</sup> ions [23]. TiO<sub>2</sub> working electrode was then immersed for 1 mint into a precursor solution of S<sup>2-</sup> containing 0.02 M of sodium sulfide nonahydrate in a solvent of methanol and water, with a ratio of 1:1 (V/V). After that, rinse again with methanol to remove excess, unwanted and dried molecules [24]. These steps constitute one complete SILAR cycle as schematically illustrated in Fig. 1 with prepared samples in the snap, while the steps can be repeated for desired number of cycles to increase the growth of QDs on TiO<sub>2</sub> film. Here we examined PbS quantum dots (QDs) using different numbers of SILAR cycles, including one, two, three, four, and five cycles. The chemical reaction of SILAR cycle for PbS is as.



### 2.5. Preparation of poly sulfide electrolyte

Poly sulfide electrolyte solution was formulated with precursor solutions comprising of 1 mol of sodium sulfide trihydrate, 1 mol of

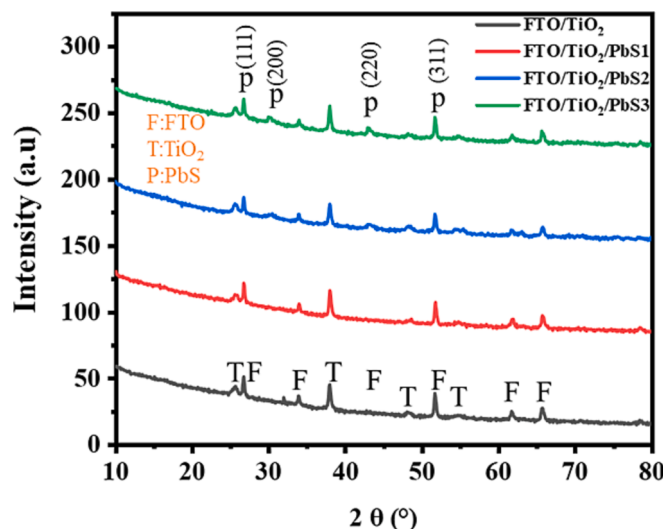


**Fig. 3.** XRD pattern of the FTO/TiO<sub>2</sub> and FTO/TiO<sub>2</sub>/PbS QDs with corresponding crystallographic planes.

Sulphur and 0.2 mol of potassium chloride in methanol/water with the ratio of 3:7 (V/V). 30 % of water is replaced with methanol to increase the solubility, enhance ionic conductivity, and reduce corrosion effect.

#### 2.6. Counter electrode setup

The preparation of the carbon counter electrode involved the coating of carbon paste onto the conductive surface of a predrilled clean FTO glass substrate using the widely recognized method of doctor blading.

#### 2.7. Fabricated device

To assemble the cells, a spot gasket with a thickness of 60 µm, specifically Meltonix 1170-60PF, was positioned over the anode layer,

overlaying titania. Subsequently, the carbon contact was placed on the spot gasket. To achieve an airtight seal, the constructed devices were subjected to a temperature of 100 °C for a duration of 20 to 30 s. After ensuring a proper seal, the polysulfide was introduced into the cells by injecting it via small holes that were drilled in the counter electrodes. Subsequently, the holes were closed and sealed using Meltonix sealing, the block diagram is shown in Fig. 2 with picture during experiment. The active area was measured to be 0.36 cm<sup>2</sup> for each cell.

#### 2.8. Sample characterizations

XRD measurements were performed on Bruker X-ray diffraction (XRD) system equipped with Cu k $\alpha$  radiation to analyze the crystal structure and crystallite size of PbS. The Shimadzu UV-1800 spectrophotometer was utilized to capture the absorption spectra of TiO<sub>2</sub> film electrodes sensitized with PbS quantum dots (QDs). The fabricated cells were subjected to photovoltaic and impedance spectroscopic studies using the Keithley 4200-SCS instrument, which featured a digital capacitance meter referred to as the model 4210-CVU. For conducting measurements under light conditions, the OAI TriSOL AM1.5G Class AAA solar simulator was employed. The power level was adjusted to 100 mWcm<sup>-2</sup> by means of the Newport Oriel photovoltaic reference cell system (Model 91150 V). IS, varying with voltage and frequency, were measured with a 30 mV RMS voltage perturbation. The frequency range was set from 5 k to 50 kHz, while the sweep voltage ranged from -1 V to +1 V.

### 3. Result and discussion

#### 3.1. XRD, surface morphology and EDX of the samples

In Fig. 3, the X-ray diffraction (XRD) results illustrate the characteristics of PbS thin films grown on FTO/TiO<sub>2</sub> via the SILAR method as a function of the 3 deposition cycles. These XRD patterns reveal prominent peaks for the anatase phase of TiO<sub>2</sub> observed at 2θ angles approximately equal to 25.3°, 37.74°, 48.03°, 53.90° and 62.79° corresponding to reflections from the (101), (004), (200), (105) and (204)

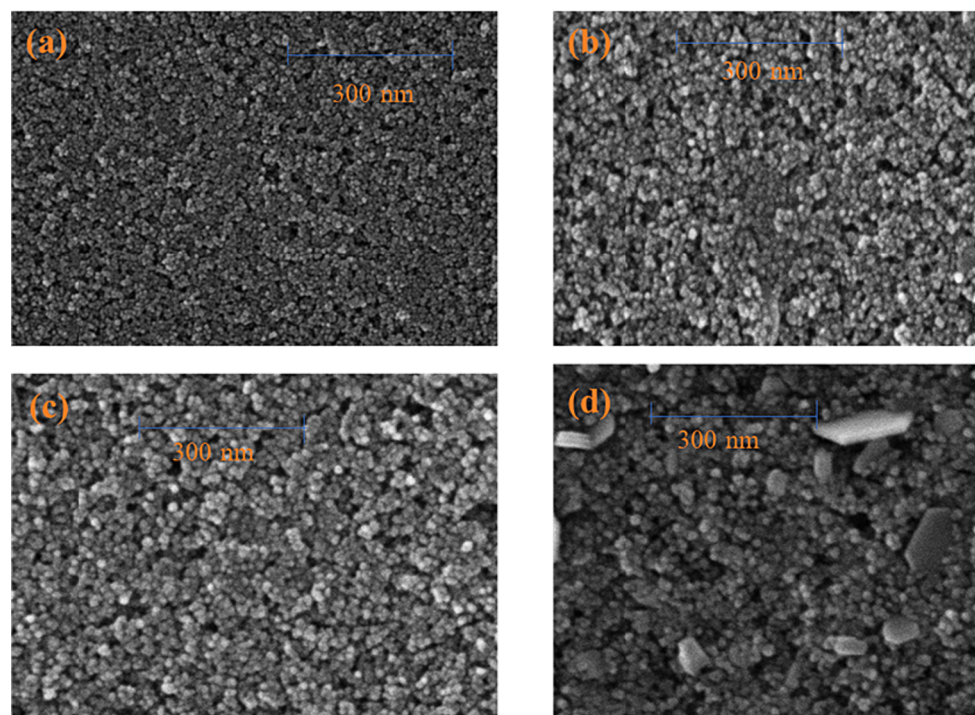


**Fig. 4.** SEM images of the (a) FTO/TiO<sub>2</sub> (b) FTO/TiO<sub>2</sub>/PbS1 (c) FTO/TiO<sub>2</sub>/PbS2 (d) FTO/TiO<sub>2</sub>/PbS3.

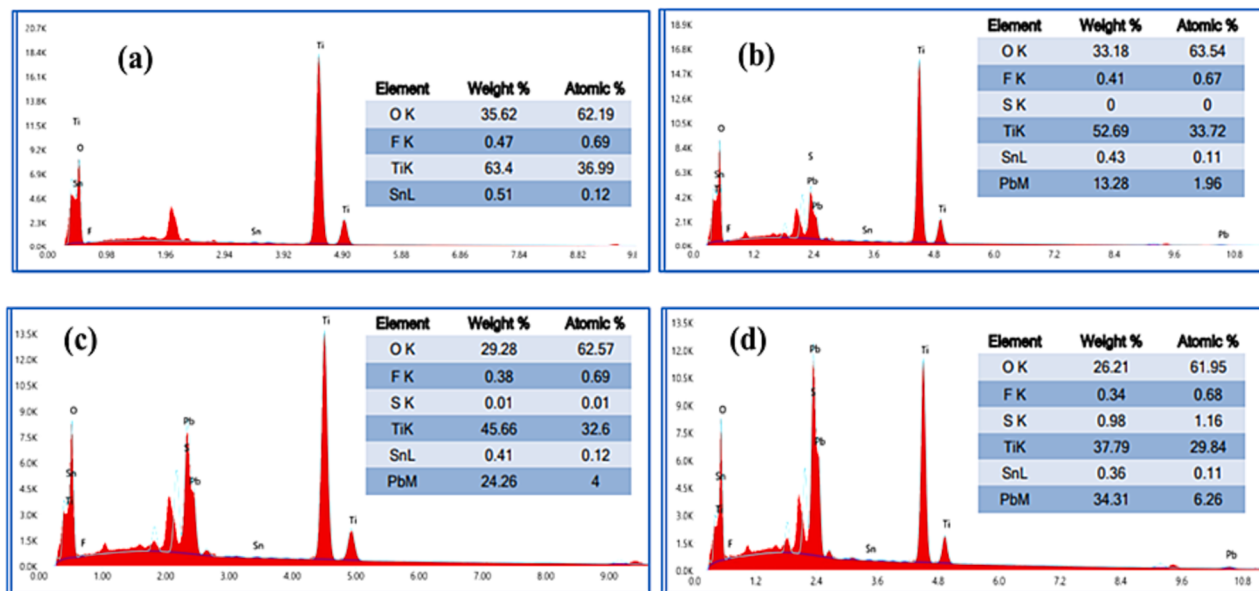


Fig. 5. EDX spectra of (a) FTO/TiO<sub>2</sub> (b) FTO/TiO<sub>2</sub>/PbS1 (c) FTO/TiO<sub>2</sub>/PbS<sub>2</sub> (d) FTO/TiO<sub>2</sub>/PbS<sub>3</sub>.

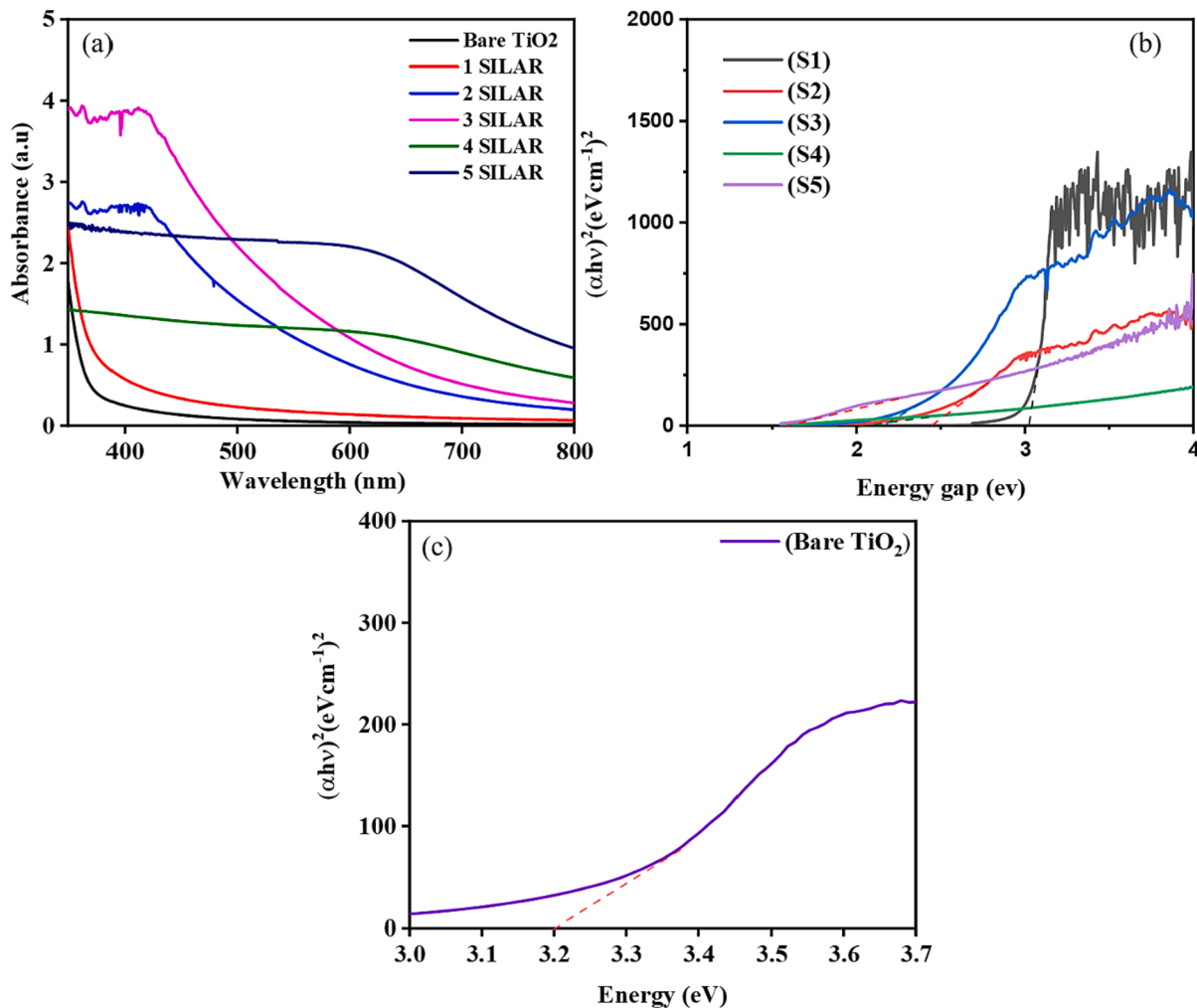


Fig. 6. (a) UV–VIS absorption spectroscopy of the bare and PbS sensitized samples (b) Tauc plot of 5 SILAR cycles (c) Tauc plot of the bare TiO<sub>2</sub>.

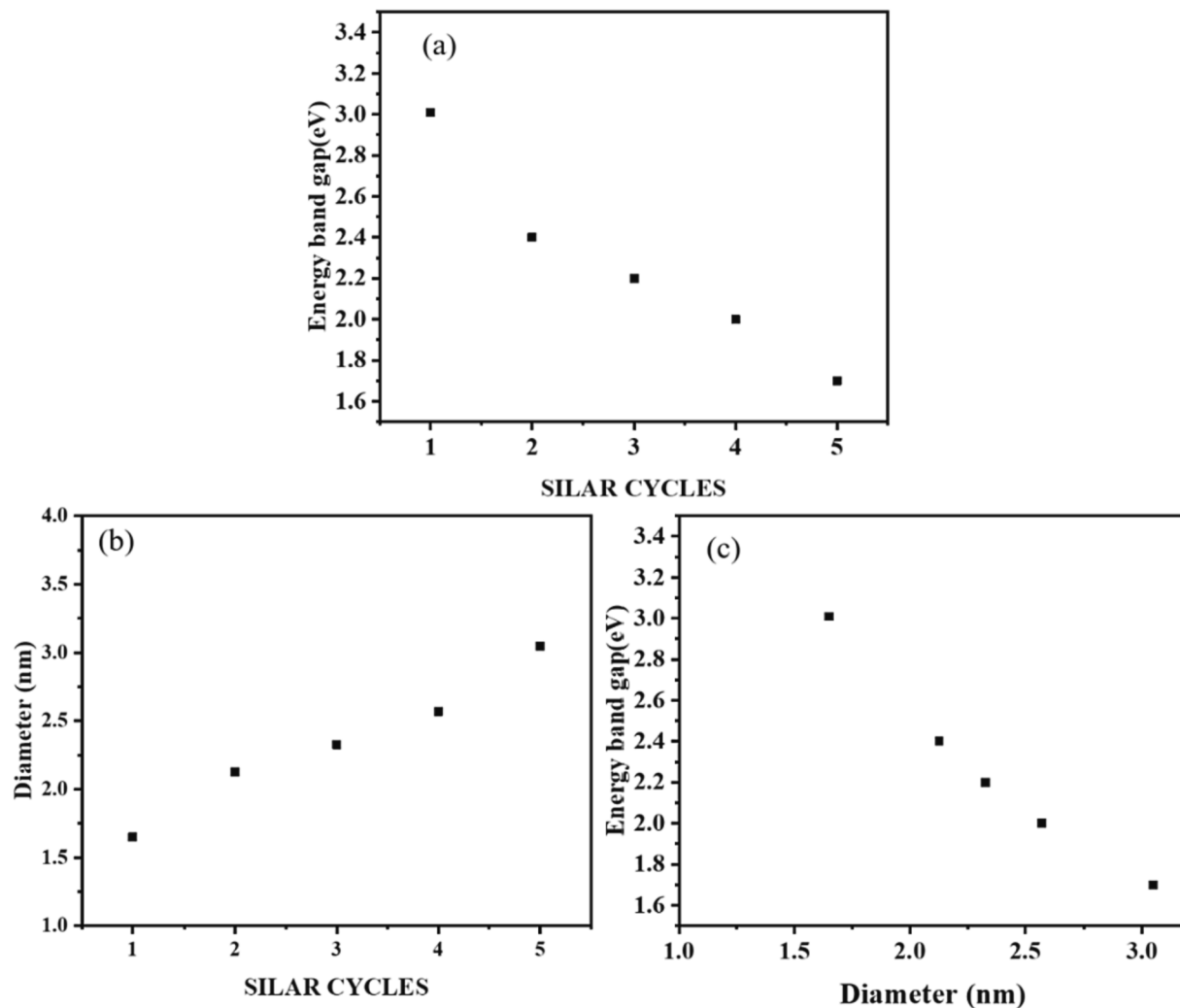


Fig. 7. (a) Energy band gap against SILAR cycles (b) diameter of QDs versus SILAR cycles (c) plot of  $E_g$  versus diameter of PbS QDs.

crystallographic planes, The peaks are consistent with (JCPDS No. 21–1272). Initially for the first SILAR cycles there are no peaks observed for PbS because the thickness of PbS is too small. But as the SILAR cycles increase to 2 and then 3, thickness increases and the observed peaks for PbS becomes more pronounced such as (111), (200), (220) and (311) at corresponding angles of 25.99°, 30.3°, 43.10° and 51.06° respectively and all the major peaks are consistent with those typically observed in the mineral Galena (PbS, PDF 00–05–0592) and JCPDS card no. 78–1901, as reported in the literature, confirming the crystalline and cubic structure of PbS [25–27]. Furthermore, the thickness of the PbS is minimal. If the SILAR cycles are further increased, the thickness increases and obtained peaks will become more prominent. With increasing SILAR cycles the thickness and Size of the PbS QD increases, resulting the decrease in the band gap [28] as discussed in UV-VIS spectra and Tauc plot. The crystallite sizes of 2.7 nm, 3.07 nm and 3.39 nm were obtained for 1 to 3 cycles respectively, using Scherrer formula as given in eq. 19, while taking the average of crystallite sizes obtained from (111), (200) and (220) planes. The crystallite size was found smaller than the Bohr exciton radius (18 nm) of PbS [29].

$$D = \frac{K\lambda}{\beta \cos\theta} \quad (2)$$

Where K is the Scherrer constant equal to 0.94,  $\lambda$  represents the wavelength of X-ray (0.154 nm), While  $\beta$  is the full width half maxima (FWHM) of the peaks in radian and the  $\theta$  indicates the half diffraction

angle. The crystallite size is slightly higher than particle size of QDs because of the PbS grown on TiO<sub>2</sub> surface [30]. Fig. 4. Shows SEM images of FTO/TiO<sub>2</sub> and FTO/PbS for 1–3 SILAR cycles at magnifications of 50 k. The SEM images reveal uniform and homogeneous surfaces with clear clusters or aggregates. The size of clusters increases with increasing SILAR cycles as can be seen in Fig. 4 (d). Furthermore, EDX spectroscopy in Fig. 5, reveals the elemental composition of the samples. In the case of PbS, with increasing SILAR cycles the atomic and weight percentage of Pb and S increases as shown in the figure.

### 3.2. UV-VIS absorption spectroscopy

Fig. 6 (a) depicts the UV-Vis absorption spectra of the TiO<sub>2</sub> electrodes in the pristine state and after being sensitized with one to five SILAR cycles of PbS quantum dots. The absorption of the photoanode intensifies as the number of SILAR cycles increases. Each spectrum associated with the TiO<sub>2</sub>/PbS electrodes showcases a wide-ranging absorption that spans from the Vis to the NIR region. The intensity of the initial three SILAR cycles exhibits a gradual increase, reaching approximately 4 arbitrary units (a.u). However, for the fourth and fifth SILAR cycles, the absorption spectrum widens. This is attributed to the bigger quantum dot size as the SILAR cycles progress, leading to a reduction in the band gap. Consequently, light absorption occurs at longer wavelengths.

The energy gap ( $E_g$ ) of PbS quantum dots and Bare TiO<sub>2</sub> (3.22 eV) can be determined through Tauc analysis as shown in Fig. 6(b) and 6(c)

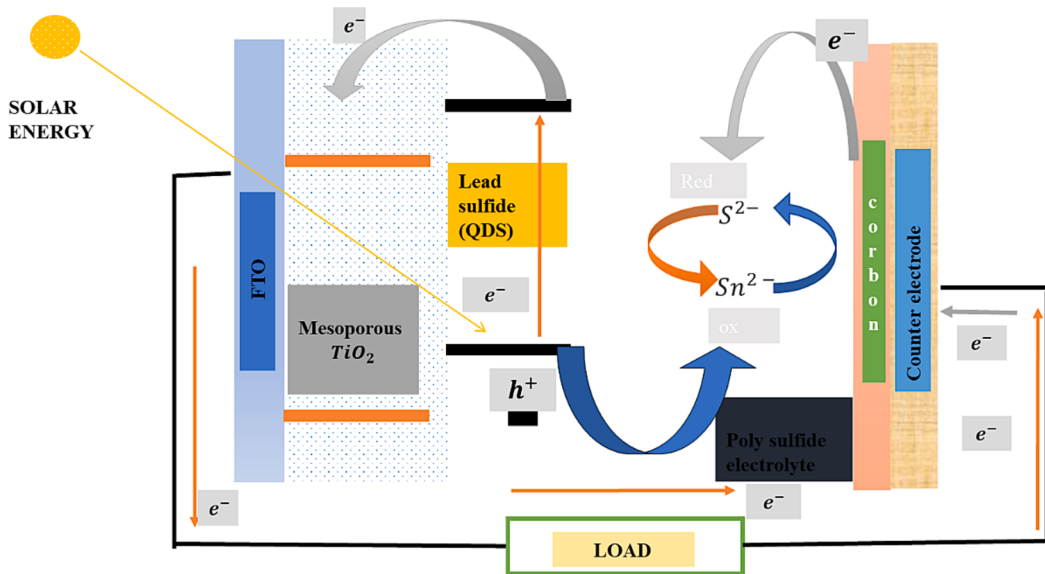


Fig. 8. Schematic representation of working principle of the fabricated PbS QDSSCs.

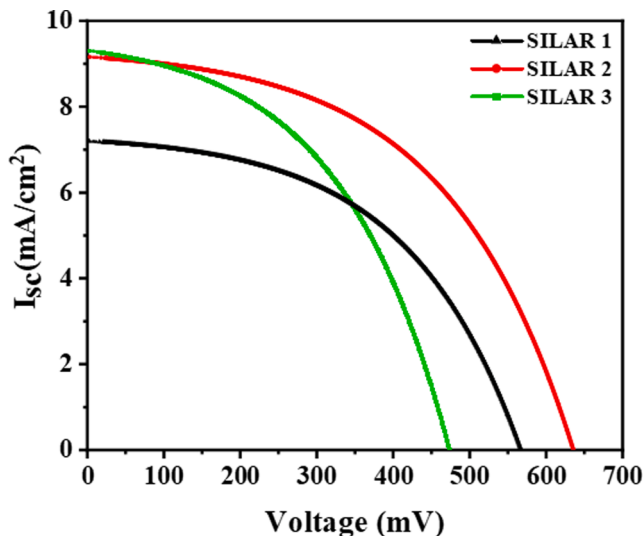


Fig. 9. J-V characteristic of fabricated devices with one, two, and three SILAR cycles.

respectively. The approximated  $E_g$  obtained from the Tauc analysis was subsequently portrayed in Fig. 6(b), which demonstrates that with the increasing number of SILAR cycles, energy band gap decreases consequently, corresponding to 3.01 eV, 2.4 eV, 2.2 eV, 2 eV, and 1.7 eV for one to five cycles, respectively as shown in Fig. 7(a). Increase in the wavelength of first excitonic absorption peaks clearly shows that size of QDs is in direct relation with number of SILAR cycles while inversely related to the energy band gap.

In a recent report, it was mentioned that the HBM, Henglein model, Brus model and the Yu equation can provide a theoretical estimated value of the nanoparticle size. In this study, the HBM model, as described by equation (3), was utilized to determine the radius of PbS quantum dots (QDs) [31].

$$R = \sqrt{\frac{h^2 E_B}{2m^*(E_O^2 - E_B^2)}} \quad (3)$$

Here,  $E_B$  is bulk band gap which is 0.41 eV,  $E_Q$  represents energy band gap of QDs and  $m^*$  denotes electron effective mass in bulk PbS where

value of  $m^*$  is 0.10  $m_e$ .

The diameter of PbS QDs was approximated to be 1.65 nm, 2.126 nm, 2.326 nm, 2.5692 nm, and 3.048 nm for one to five SILAR cycles respectively as illustrated in Fig. 7(b). Similarly, Fig. 7(c) depicted quantum dot size in diameter against the energy band gap, clearly demonstrating inverse relation. Furthermore, the estimated size of nanoparticles is less than the Bohr exciton radius of PbS that is 18 nm, thus quantum confinement effect occurs [29].

### 3.3. Photovoltaic measurements

The operational concept can be readily understood by referring to the schematic diagram depicted in Fig. 8. When light illuminates lead sulfide quantum dots, it triggers the generation of electron-hole pairs. The electrons migrate towards the electron transport layer ( $TiO_2$ ), while the holes move towards the polysulfide electrolyte. This charge separation establishes a potential difference, resulting in the open-circuit voltage ( $V_{oc}$ ) of the system. Subsequently, the electrons flow into the outer circuit to perform useful work and are recollected by the carbon electrode. The role of the electrolyte is to facilitate efficient electron transfer between the counter electrode and PbS quantum dots while engaging in redox reactions to ensure the completion of the circuit. The I-V characteristics of the fabricated PbS QDSSCs in Fig. 9, demonstrate the optimal number of current densities of 7.04 mA/cm<sup>2</sup>, open circuit voltage of 572 mV, fill factor (FF) of 0.33, and a power conversion efficiency of 1.33 % for one SILAR cycle. Lower performance is observed when employing one SILAR cycle, due to a limited quantity of PbS in the device, absorption primarily at shorter wavelengths because of higher band gap, potentially hindering the efficient transfer of electrons to the conduction band of  $TiO_2$ . Consequently, the maximum current ( $I_{max}$ ) and maximum voltage ( $V_{max}$ ) achievable by the device are reduced. Higher power conversion efficiency of 2.07 % was attained for 2 SILAR cycles, because of the compatible band gap and appropriate quantum dot size in relation to  $TiO_2$ , facilitating efficient electron transfer. Moreover, at this band gap, the quantum dots are capable of absorbing light at both shorter and longer wavelengths. Additionally, the size of the quantum dots may be suitable for electrolyte penetration into the quantum dots. However, when the number of SILAR cycles exceeds two, such as in the case of three cycles, it leads to a decrease in efficiency. The effectiveness of QDSSCs diminishes as the number of SILAR cycles increases, resulting in larger quantum dots (QDs) sizes lower band gap and subsequent aggregation. This aggregation of QDs adversely affects the

**Table 1**

Comparative photovoltaic performance of three fabricated devices along with reported data in terms of performance parameters.

SILAR cycles	$J_{sc}$ (mA/cm <sup>2</sup> )	$V_{oc}$ (mV)	FF	Efficiency (%)	$P_{max}$ (mW)	$R_s$ ( $\Omega$ . cm <sup>2</sup> )	$R_{sh}$ ( $\Omega$ . cm <sup>2</sup> )
1	7.04	571	0.33	1.33	0.471	7.33	454.4
2	9.03	642	0.37	2.07	0.79	6.53	705.8
3	9.28	482	0.36	1.63	0.59	6.65	392.7
Ref. [1]	16.3	370	0.29	1.79	—	—	—
Ref. [33]	11.2	390	0.47	1.92	—	—	—

average electronic coupling and increases the distance between TiO<sub>2</sub> and the quantum dots, as observed by Kern and Watson in 2014. Consequently, the reduced charge transfer between the quantum dots and TiO<sub>2</sub> leads to a decline in the overall performance of the QDSSC. The lower  $V_{oc}$  observed in case of three SILAR cycles is attributed to the lower band gap resulting in recombination of electron-hole pairs. The configuration of the I-V graph is responsive to either the series resistance ( $R_s$ ) or the shunt resistance ( $R_{sh}$ ). For low values of  $R_s$ , a substantial current pass through the cell, even at low applied voltage, while the considerable shunt resistance  $R_{sh}$  experiences photocurrent leakages. Achieving a high fill factor (FF) for efficient power conversion requires minimizing the series resistance (ideally approaching zero) and large shunt resistance (approaching infinity) [32].  $R_s$  and  $R_{sh}$  can be determined from the I-V graph as given in eq.4 and eq.5 respectively. For  $R_{sh}$  locate the point of maximum current at  $V = 0$  and a reference point close

to the short circuit current point, the inverse of the slope yield  $R_{sh}$ . Similarly, for  $R_s$  locate the point at  $V = V_{oc}$  and slightly close to  $V_{oc}$ , the inverse of the slope at these points provides  $R_s$ . The more flattened curve demonstrates the lowest series resistance and a large  $R_{sh}$ . Thus, obtained enlarge FF and PCE as in case 2 SILAR cycles. Table 1, comparatively determine the associated parameters and efficiency for each SILAR cycle and with the reported literature.

$$R_{sh} = \frac{\Delta V}{\Delta I} at V = 0 \quad (4)$$

$$R_s = \frac{\Delta V}{\Delta I} at V = V_{oc} \quad (5)$$

### 3.4. Impedance spectroscopy

Impedance spectroscopy (IS) is a widely employed and utilized characterization technique operating in Alternating current (AC) that holds significant reliability while studying photovoltaic devices and electrochemical systems [34]. Nevertheless, when it comes to characterizing emerging photovoltaics like DSSCs, PSCs and QDSSCs, employing impedance spectroscopy presents unique challenges. These challenges include addressing interfacial degradation concerns [35], accounting for unconventional material properties, and validating simulated data through testing [36]. During impedance spectroscopy (IS) measurements, a voltage (V) is applied across the solar cell at a specific frequency ( $f_s$ ). The supplied voltages and frequencies modify the behavior of the device, and these modifications can be observed and analyzed from the impedance spectra [37]. Hence, to acquire a deeper

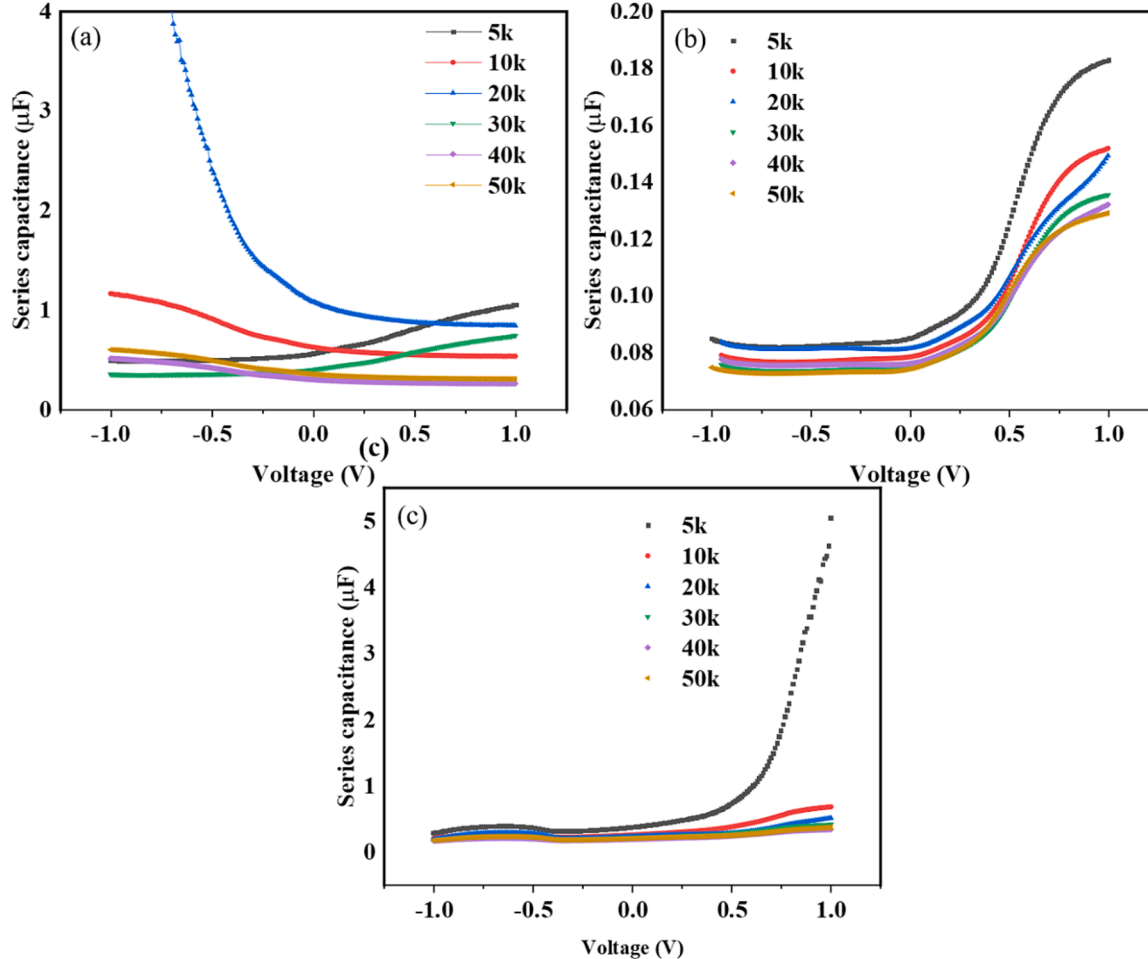
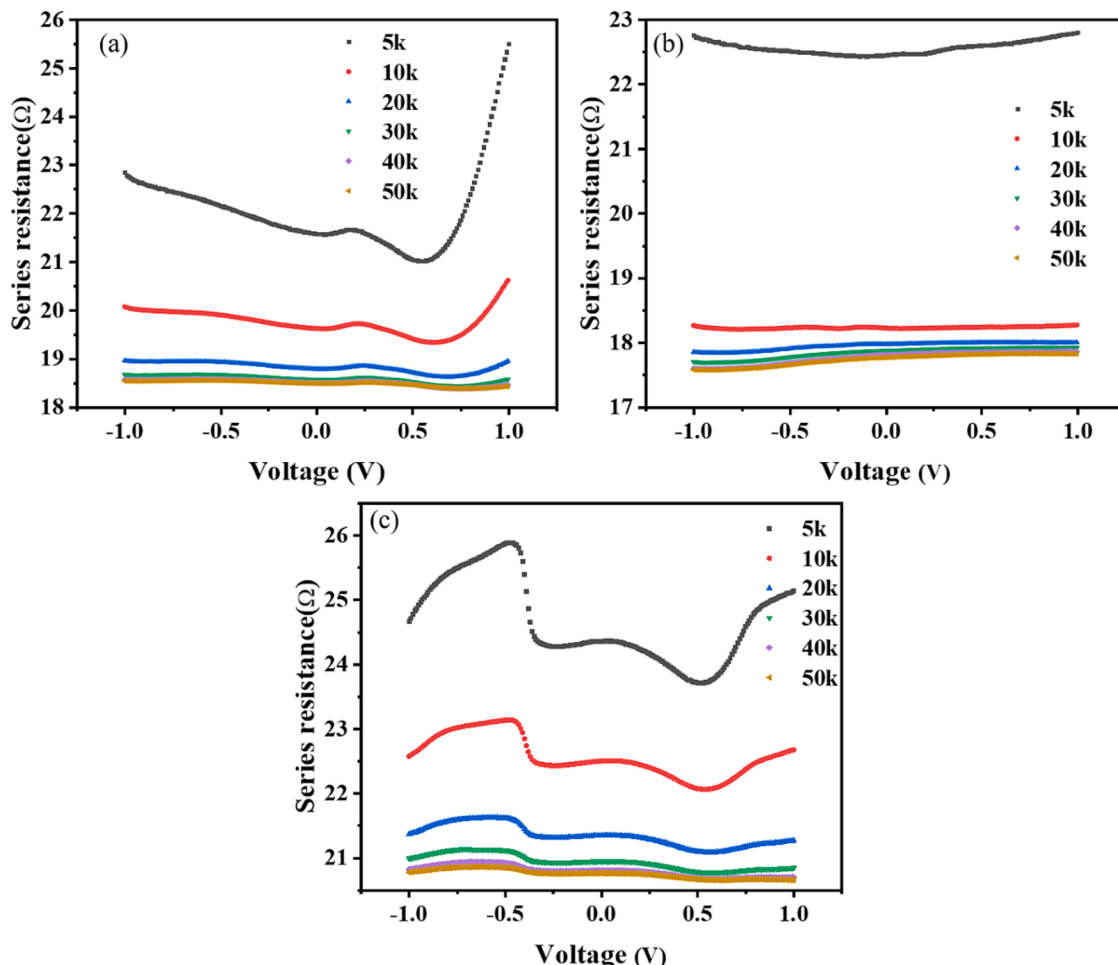


Fig. 10. Series capacitance vs voltage ( $C_s$ -V) recorded at frequencies between 5 kHz and 50 kHz for (a) one SILAR cycle (b) two SILAR cycles (c) three SILAR cycles.



**Fig. 11.** Series resistance against bias voltage ( $R_s$ -V) curves at different frequencies for (a) 1 SILAR (b) 2 SILAR (c) 3 SILAR.

understanding of the charge kinetics in quantum dot-sensitized solar cells (QDSSCs), which can help in optimizing different interfaces and components of the device for improved and stable performance, it is imperative to study the impedance spectra dependent on voltage (V) and frequency (F). In this study, impedance spectroscopy was employed to examine series capacitance–voltage ( $C_s$ -V), and series resistance–voltage ( $R_s$ -V) characteristics for the assembled devices with one, two and three SILAR cycles. The cell comprises various capacitances distributed across multiple layers of solar cells, including interfaces. These capacitances enable the accumulation of charges at different potentials. The collective impact of these individual capacitances is referred to as series capacitance. Similarly, series resistance refers to total resistance encountered by the electron while moving through the interfaces, cell contacts and other elements of the circuit. Fig. 10(a), (b) and (c) illustrate series capacitance versus bias voltage ( $C_s$ -V) at different frequencies ranging from 5 k to 50 kHz. Initially at low bias voltage the capacitance remains almost constant, but as the voltage exceeds 0.0 V, capacitance shows voltage dependency and increases exponentially at fixed frequency attributed to its shrink depletion region. Additionally, with increasing frequencies the value of capacitance is decreasing, this is because the absorber traps do not effectively capture the fast-moving waves of energy, thus reducing the effective charge and hence resulting in lower device capacitance. The lowest series capacitance was observed for 2 SILAR cycles. Likewise, Fig. 11(a), (b) and (c) demonstrate series resistance against bias voltage ( $R_s$ -V) at different frequencies in the range between 5 k and 50 kHz. There is no momentous change observed in resistance with applied voltage for two SILAR cycles as shown Fig. 11(b). However, in the case of Fig. 11(a) and (c) series

resistance raises with further enhancement in voltage. Furthermore, it is clear from the graphs that  $R_s$  shows strong dependency on frequency hence high resistance is witnessed for 5 kHz, while low resistance was viewed when frequency escalates to 50 kHz.

#### 4. Conclusion and future perspectives

The photovoltaic performance of PbS QDSSCs was investigated by employing the SILAR deposition method. The impact of varying deposition cycles (ranging from one to three cycles) on the effectiveness of PbS QDSSCs was emphasized. UV-VIS spectroscopy shows absorption spectra for each cycle. Best performance of 2.07 % efficiency was obtained in the case of 2 SILAR Cycles, attributed to its compatible QDs size, band gap and low series resistance and capacitance resulting in efficient penetration of electrolyte, transfer of electron and low recombination. The estimated energy band gap and size of QDs were found to be 3.01 eV, 2.4 eV, 2.2 eV, 2 eV, 1.7 eV and 1.65 nm, 2.126 nm, 2.326 nm, 2.5692 nm, and 3.048 nm for one to five SILAR cycles, respectively. Furthermore, based on observations, it was found that the increasing SILAR cycles lead to increase in QDS size and decrease in energy band gap. Hence poly sulfide and carbon can be utilized as electrolyte and counter electrode for fabricating low-cost solar cell with satisfactory photovoltaic performance. The utilization of a poly sulfide electrolyte along with a carbon counter electrode result in improved proficiency in QDSSCs ascribed to facilitate efficient electrochemical reactions, exhibit high electron conductivity, ensure stability as no side reactions and corrosion occurs, and offer cost-effectiveness. Moreover, the outcomes can be further boosted via co-sensitization of PbS with other QDs,

passivating layers and counter electrodes with high catalytic activity.

## CRediT authorship contribution statement

**Zafar Ali:** Writing – original draft, Software, Project administration, Methodology, Data curation, Conceptualization. **Muhammad Hassan Sayyad:** Supervision. **Ahmad Ali:** Writing – review & editing. **Mujeeb ur Rahman:** Writing – review & editing. **Nadia Anwar:** Writing – review & editing. **Sajid Khan:** Writing – review & editing.

## Declaration of competing interest

The authors declare that they have no known competing financial interests or personal relationships that could have appeared to influence the work reported in this paper.

## Data availability

Data will be made available on request.

## Acknowledgement

We would like to acknowledge the center of emerging solar cell technology (CESCT) faculty of engineering sciences for providing the lab facilities.

## Funding

This research did not receive any specific grant from funding agencies in the public, commercial, or not-for-profit sectors.

## References

- [1] W. Yindeesuk, P. Tusamalee, F. Liu, T. Toyoda, and Q. Shen, "Effect of SILAR techniques on photovoltaic properties of PbS quantum dot sensitized solar cells," in *Journal of Physics: Conference Series*, 2018, vol. 1144, no. 1, p. 012144; IOP Publishing.
- [2] L.S. Lau, C.K. Choong, Y.K. Eng, Investigation of the environmental Kuznets curve for carbon emissions in Malaysia: do foreign direct investment and trade matter? *Energy Policy* 68 (2014) 490–497.
- [3] J. Perlin, Silicon solar cell turns 50, National Renewable Energy Lab, Golden, CO, (US)2004..
- [4] J. Melskens, et al., Concepts and prospects of passivating contacts for crystalline silicon solar cells, in: In 2015 IEEE 42nd Photovoltaic Specialist Conference (PVSC), IEEE, 2015, pp. 1–6.
- [5] G. Strobl, et al., European roadmap of multijunction solar cells and qualification status, in: In 2006 IEEE 4th World Conference on Photovoltaic Energy Conference, vol. 2, IEEE, 2006, pp. 1793–1796.
- [6] C.W. Tang, Two-layer organic photovoltaic cell, *Appl. Phys. Lett.* 48 (2) (1986) 183–185.
- [7] B. O'regan, M.J.n. Grätzel, A low-cost, high-efficiency solar cell based on dye-sensitized colloidal TiO<sub>2</sub> films, *Nature* 353 (6346) (1991) 737–740.
- [8] T. Yang, et al., One-stone-for-two-birds strategy to attain beyond 25% perovskite solar cells, *Nat. Commun.* 14 (1) (2023) 839.
- [9] P.V. Kamat, Quantum dot solar cells. Semiconductor nanocrystals as light harvesters, *J. Phys. Chem. C* 112 (48) (2008) 18737–18753.
- [10] S. Rühle, M. Shalom, A.J.C. Zaban, Quantum-dot-sensitized solar cells, *ChemPhysChem* 11 (11) (2010) 2290–2304.
- [11] Q. Shen, K. Katayama, T. Sawada, S. Hachiya, T.J.C.P.L. Toyoda, Ultrafast carrier dynamics in PbS quantum dots, *Chem. Phys. Lett.* 542 (2012) 89–93.
- [12] M.C. Hanna, A.J. Nozik, Solar conversion efficiency of photovoltaic and photoelectrolysis cells with carrier multiplication absorbers, *J. Appl. Phys.* 100 (7) (2006) 074510.
- [13] N. Guijarro, J.M. Campiña, Q. Shen, T. Toyoda, T. Lana-Villarreal, R. Gómez, Uncovering the role of the ZnS treatment in the performance of quantum dot sensitized solar cells, *Phys. Chem. Chem. Phys.* 13 (25) (2011) 12024–12032, <https://doi.org/10.1039/C1CP20290A>.
- [14] C. Ratanatawanate, C. Xiong, K.J. Balkus Jr, Fabrication of PbS quantum dot doped TiO<sub>2</sub> nanotubes, *ACS Nano* 2 (8) (2008) 1682–1688.
- [15] A. Braga, S. Giménez, I. Concina, A. Vomiero, I. Mora-Seró, Panchromatic sensitized solar cells based on metal sulfide quantum dots grown directly on nanostructured TiO<sub>2</sub> electrodes, *J. Phys. Chem. Lett.* 2 (5) (2011) 454–460.
- [16] Y. Jiang, et al., Boosting the Open Circuit Voltage and Fill Factor of QDSSCs Using Hierarchically Assembled ITO@Cu2S Nanowire Array Counter Electrodes, *Nano Lett.* 15 (5) (2015/05/13 2015) 3088–3095.
- [17] C.V.M. Gopi, M. Venkata-Haritha, S.-K. Kim, S.S. Rao, D. Punnoose, H.-J. Kim, "Highly efficient and stable quantum dot-sensitized solar cells based on a Mn-doped CuS counter electrode," *RSC Adv.* 5 (4) (2015) 2963–2967, <https://doi.org/10.1039/C4RA12968G>.
- [18] D.B. Salunkhe, S.S. Gargote, D.P. Dubal, W.B. Kim, B.R. Sankapal, Sb2S3 nanoparticles through solution chemistry on mesoporous TiO<sub>2</sub> for solar cell application, *Chem. Phys. Lett.* 554 (2012/12/03/ 2012.) 150–154.
- [19] C.V.M. Gopi, et al., "One-step synthesis of solution processed time-dependent highly efficient and stable PbS counter electrodes for quantum dot-sensitized solar cells," *RSC Adv.* 5 (130) (2015) 107522–107532, <https://doi.org/10.1039/CSRA22715A>.
- [20] B. Pandit, S.A. Pande, B.R. Sankapal, Facile SILAR processed Bi2S3: PbS solid solution on MWNTs for high-performance electrochemical supercapacitor, *Chinese J. Chem.* 37 (12) (2019) 1279–1286.
- [21] P.R. Nikam, P.K. Baviskar, J.V. Sali, K.V. Gurav, J.H. Kim, B.R.J.C.I. Sankapal, SILAR coated Bi2S3 nanoparticles on vertically aligned ZnO nanorods: synthesis and characterizations, *Ceram. Int.* 41 (9) (2015) 10394–10399.
- [22] C.V. Gopi, et al., One-step synthesis of solution processed time-dependent highly efficient and stable PbS counter electrodes for quantum dot-sensitized solar cells, *RSC Adv.* 5 (130) (2015) 107522–107532.
- [23] B. Shi, Y. Qi, L. Tian, L. Liu, The enhanced photoelectrochemical performance of PbS/ZnS quantum dots co-sensitized CdSe nanorods array heterostructure, *Mater. Sci. Semiconductor Process.* 98 (2019/08/01/ 2019.) 7–12.
- [24] B. Shi, Y. Qi, L. Tian, Fabrication of Ag2S quantum dots sensitized CdSe photoelectrodes and its photoelectric performance, *Mater. Chem. Phys.* 240 (2020/01/15/ 2020) 122177.
- [25] C. Pérez-García, S. Meraz-Dávila, G. Arreola-Jardón, F. de Moure-Flores, R. Ramírez-Bon, Y.J.M.R.E. Vorobiev, Characterization of PbS films deposited by successive ionic layer adsorption and reaction (SILAR) for CdS/PbS solar cells application, *Mater. Res. Express* 7 (1) (2020) 015530.
- [26] V. Jyothilakshmi, N. Bhabhina, M. Dharsana, S.J.M.T.P. Swaminathan, Wet chemical synthesis of lead sulfide nanoparticles and its application as light harvester in photovoltaic cell, *Mater. Today: Proc.* 33 (2020) 2125–2129.
- [27] Y. Li, et al., Efficient PbS/CdS co-sensitized solar cells based on TiO<sub>2</sub> nanorod arrays, *Nanoscale Res. Lett.* 8 (2013) 1–7.
- [28] R.S. Mane, B.R. Sankapal, C.D. Lokhande, Thickness dependent properties of chemically deposited As2S3 thin films from thioacetamide bath, *Mater. Chem. Phys.* 64 (3) (2000) 215–221.
- [29] J.-W. Lee, et al., Quantum-dot-sensitized solar cell with unprecedentedly high photocurrent, *Sci. Rep.* 3 (1) (2013) 1050.
- [30] N. Wichaiyo, M. Kitwan, Q. Shen, W. J. C. A. S. Yindeesuk, and TECHNOLOGY, "The Effect of PbS Colloidal Quantum Dots with CdS and ZnS Coating on Photovoltaic Properties," *CURRENT APPLIED SCIENCE AND TECHNOLOGY*, pp. 10.55003/cast. 2022.02. 23.011 (14 pages)-10.55003/cast. 2022.02. 23.011 (14 pages), 2023.
- [31] S.M. Ali, M. Aslam, W. Farooq, A. Fatehmulla, M.J.M. Atif, Assembly of CdS quantum dots onto hierarchical TiO<sub>2</sub> structure for quantum dots sensitized solar cell applications, *Materials* 8 (5) (2015) 2376–2386.
- [32] A. Gholizadeh, A. Reyhani, P. Parvin, S.Z. Mortazavi, "Efficiency enhancement of ZnO nanostructure assisted Si solar cell based on fill factor enlargement and UV-blue spectral down-shifting," *J. Phys. D Appl. Phys.* 50 (04/03 2017.) 11.
- [33] S. Hachiya, Q. Shen, T. J. J. o. A. P. Toyoda, "Effect of ZnS coatings on the enhancement of the photovoltaic properties of PbS quantum dot-sensitized solar cells," *J. Appl. Phys.* vol. 111, no. 10, (2012).
- [34] E. J. T. J. o. P. C. C. Von Hauff, "Impedance spectroscopy for emerging photovoltaics," *J. Phys. Chem. C*, vol. 123, no. 18, pp. 11329–11346, 2019.
- [35] A. Guerrero, et al., Interfacial degradation of planar lead halide perovskite solar cells, *ACS Nano* 10 (1) (2016) 218–224.
- [36] A. Braña, E. Fornié, N. López, and B. García, "High efficiency Si solar cells characterization using impedance spectroscopy analysis," in *Journal of Physics: Conference Series*, 2015, vol. 647, no. 1, p. 012069: IOP Publishing.
- [37] H. Lee, C. Lee, H.-J.-J.-M. Song, Influence of electrical traps on the current density degradation of inverted perovskite solar cells, *Materials* 12 (10) (2019) 1644.